Journal of Nuclear Materials 493 (2017) 246–254

Contents lists available at ScienceDirect

Journal of Nuclear Materials

journal homepage: www.elsevier.com/locate/jnucmat

On the damage and fracture of nuclear graphite at multiple length-scales

Dong Liu [a, d, *], Ken Mingard [b], Oliver T. Lord [c], Peter Flewitt [d]

[a] Department of Materials, University of Oxford, Oxford, OX1 3PH, UK
[b] National Physical Laboratory, Teddington, TW11 0LW, UK
[c] School of Earth Sciences, University of Bristol, Bristol, BS8 1RJ, UK
[d] HH Wills Physics Laboratory, School of Physics, University of Bristol, Bristol, BS8 1TL, UK

ARTICLE INFO

Article history:
Received 7 April 2017
Received in revised form
10 June 2017
Accepted 15 June 2017
Available online 17 June 2017

Keywords:
Micro-mechanical testing
Multiple length-scales
Nano-indentation
Elastic modulus
Graphite

ABSTRACT

Gilsocarbon graphite, as a neutron moderator and load-bearing component in the core of the UK fleet of Advanced Gas-Cooled Reactors, possesses complex microstructural features including defects/pores over a range of length-scales from nanometres to millimetres in size. As a consequence, this material exhibits different characteristics when specimens of different length-scale are deformed. In this work, the deformation and fracture of this material have been characterised using *in situ* methods for specimens of micrometre size (meso-scale) and the results are then compared with those measured one length-scale smaller, and those at the macro-scale. At the micro-scale, sampling a volume of material ($2 \times 2 \times 10$ μm) excludes micro- and macro-size pores, the strength was measured to be as high as 1000 MPa (an elastic modulus of about 67 GPa). When the specimen size is increased by one order of magnitude to the meso-scale, the strength is reduced to about 100 MPa (an elastic modulus of about 20 GPa) due to the inclusion of micro-size pores. For larger engineering-size specimens that include millimetre-size pores, the strength of the material averages about 20 MPa (an elastic modulus of about 11 GPa). This trend in the data is discussed and considered in the context of selecting the appropriate data for relevant multi-scale modelling.

1. Introduction

Commercial graphites such as those used as moderators in the reactor cores of civil nuclear power plants have quasi-brittle characteristics [1–3]. In general, these materials are multi-phase, aggregated and porous, and the overall microstructures have been considered to cover multiple length-scales [4–6]. In the case of as-manufactured Gilsocarbon graphite used in the UK fleet of Advanced Gas-cooled Reactors (AGRs), there is about 20 vol% porosity consisting of pores ranging from nanometres to millimetres in diameter [6,7]. This porosity is distributed between the filler particles (Gilsonite coke) and the binder phase which comprises graphitised ground fine filler particles and coal tar pitch. Furthermore, the microstructure of this material is modified by neutron irradiation and radiolytic oxidation in the CO_2 gas environment of the AGRs. This leads to an overall reduction in strength, distortion and potential fracture of the graphite bricks that make up the reactor core [3,7]. Therefore, it is of paramount importance to understand the deformation and fracture of this material prior to irradiation and after service. To measure the physical and mechanical properties, irradiated graphite samples are removed periodically either from the core bricks using trepanning or as surveillance samples, limiting the sample sizes that are available for laboratory tests. As a consequence, mechanical property measurements obtained from small-scale testing have been recognised as advantageous for the investigation of such radioactive materials [8–10].

There are various experimental configurations available for micro-mechanical testing including nano-indentation, micro-pillar compression and micro-cantilever bending [11–14]. Since nuclear graphites have complex and porous microstructures, *ex situ* testing such as nano-indentation does not provide sufficient information for the interpretation of the load-displacement behaviour. Hence we explore this aspect in this paper, for Gilsocarbon graphite

* Corresponding author. Department of Materials, University of Oxford, Oxford, OX1 3PH, UK.
E-mail address: dong.liu@materials.ox.ac.uk (D. Liu).

http://dx.doi.org/10.1016/j.jnucmat.2017.06.021
0022-3115/

specimens, using *ex situ* nano-indentation and compare the results with *in situ* testing. However, even with *in situ* testing, there is a need to be particularly aware of the correlation between the micro-size specimens and the local microstructure of the material. As Liu *et al* [7] pointed out, at small length-scales, test data can vary significantly with specimen size: when measuring at the micro-scale, e.g. a specimen size of 2 × 2 × 10 μm, there is a large scatter of the measured properties, such as the elastic modulus and strength, due to the heterogeneity of the local microstructure. Even at this scale, the selection of cantilever beam specimens would not exclude all the pores - especially those nano-size pores visible in ion-milled cross-sections and transmission electron microscopy. Therefore, Liu *et al* [7] emphasized that the highest value measured using these small specimens represents the lower bound of the 'true' properties of the graphite material excluding the micro- and macro-pores.

In this paper, larger cantilever beam specimens, typically one order of magnitude larger than those studied by Liu *et al* [7], were investigated. These larger cantilever beam test specimens aim to include a number of micro-scale pores (typically around 1–2 μm equivalent spherical diameter) and thus provide an average of the mechanical properties of the graphite material at this intermediate (meso-) scale. The measured data are compared across the length scale range and discussed with respect to their importance for input to computer models.

2. Materials and experiments

2.1. Materials

The polygranular Gilsocarbon graphite (IM1-24 grade) material was supplied by EDF Energy. It is one of the nuclear-grade graphites used in the core of the UK AGR fleet. A relatively uniform distribution of filler particles is achieved in this graphite by vibrational moulding. As a result, when either the strength or the coefficient of thermal expansion is measured in samples that have been machined either along or normal to the moulding direction, a small anisotropy ratio of 1:1.1 is measured. Hence macroscopically the material is effectively isotropic with respect to mechanical properties such as elastic modulus (11–12 GPa), tensile strength (19–20 MPa) and flexural strength (about 26 MPa) [1,2,6,15]. An optical image of the overall structure is shown in Fig. 1a including the filler particles, binder phase and pores. In addition, to emphasize the multi-scale nature of the microstructure of this Gilsocarbon graphite, a scanning electron microscope (SEM) secondary electron image of a focussed ion beam (FIB) milled cross-section is shown in Fig. 1b. Micro- and sub-micrometre pores/cracks are distributed in the filler particles and matrix. The total porosity in this graphite is measured to be about 20 vol% [7]. For the macro-pores this is about 4–6 area% and about 7 vol% (with the diameter between a few micrometre to about several hundred micrometre) from SEM/optical measurements and 3D X-ray computed tomography scans respectively. Nano-scale Mrozowski cracks are also present from transmission electron microscope observations but their actual volume fraction is difficult to quantify due to the small area/volume examined. More detailed descriptions of the microstructure of the same grade, from different billets can be found elsewhere [1,5,10,15–18].

2.2. Mechanical testing

The various arrangements used to undertake mechanical testing across several length-scales are shown in Fig. 2. The first (Fig. 2a) is an *ex situ* nano-indentation test on a specimen surface using a G200 nano-indenter with a Berkovich tip (UKAEA Culham, UK). Following these *ex situ* tests, *in situ* nano-indentation was undertaken at the National Physical Laboratory, UK, using an Asmec nano-indenter (Zwick/Roell) located within a Zeiss AURIGA crossbeam FIB-SEM system (Fig. 2b). In both cases, the indentation was calibrated against a fused silica standard prior to the experiments.

Nano-indentation is easy to carry out and requires little sample preparation. However, the complex stress state under the indenter makes it more difficult to derive strength data. Therefore, micro-mechanical testing on either FIB milled or laser ablation fabricated micro-scale specimens was adopted to obtain deformation and fracture information for this Gilsocarbon graphite. Two arrangements are used for this type of test. Fig. 2c shows one type using a square section cantilever beam (~2 × 2 × 10 μm) made by focused Ga^+ ion beam milling and loaded to fracture *in situ* by a customised force measurement probe installed on a micro-manipulator (Kleindiek Nanotechnik GmbH) within an FEI Helios NanoLab 600i Dualbeam workstation. The detailed fabrication process for the cantilever *samples* can be found in Ref. [7]. Briefly, the specimens were prepared in two steps. Firstly, rectangular slots were gallium ion milled at a separation related to the final size of the specimen with the incident ion beam inclined at 45 deg to the sample. This was followed by repeat milling at 90 deg to the first slot direction to produce a square section specimen; a low incident ion current of 2.7 nA was used to produce a final specimen with minimum ion damage. The force measurement system outputs the load applied to a resolution of 0.01 μN and displacement was measured from SEM images. The side surface of the cantilever beam can be viewed continuously by SEM imaging as it is deformed, allowing displacement to be measured while the applied load is recorded from the loading probe (Fig. 2c). This loading system can apply a maximum load of 360 μN and therefore limits the section size of the specimen to a few micrometres. This is the setup adopted by Liu *et al.* [7], and the details regarding the potential effects from ion implantation, loading probe sliding during a test and analytical errors can be found in Ref. [7] which includes data for comparison with the meso-size test results described here. Meso-scale cantilever specimens with a triangular cross-section as those used by Armstrong *et al.* [12] were tested by the second arrangement, shown in Fig. 2d. These cantilevers are one order of magnitude larger in size (~20 × 20 × 150 μm) compared with the small cantilevers and were machined by ultra-violet laser ablation when FIB milling is not feasible due to the large dimensions. Raman spectroscopy was used to check the sample surface prior to the laser ablation and after to confirm the absence of laser heat induced damage on the test cantilevers by comparing the intensity ratio between the D peak (~1350 cm^{-1}) and G peak (~1580 cm^{-1}). Subsequently, these larger cantilever beam specimens were loaded to fracture at NPL using an *in situ* Asmec nano-indenter (Zwick/Roell) fitted with a flat tip (diameter of 5 μm), see Fig. 2d. Five cantilever specimens were tested, with each loaded under displacement control through several cycles prior to fracture. The cross-sectional size of each specimen has been examined subsequently by FIB milling within a Helios NanoLab 600i workstation.

3. Results

3.1. Indentation

Ex situ indentation was carried out in terms of maps in groups of 20, 16 and 24 measurements under load control (100 mN) with a loading rate of 0.05 mN/s at evenly spaced points (every 100 μm). One set of the load-displacement curves is shown in Fig. 3a where the shape of the curve and displacement into the specimen surface (from about 3000 nm to 9000 nm) changes over a large range from location to location. The elastic modulus measured from the

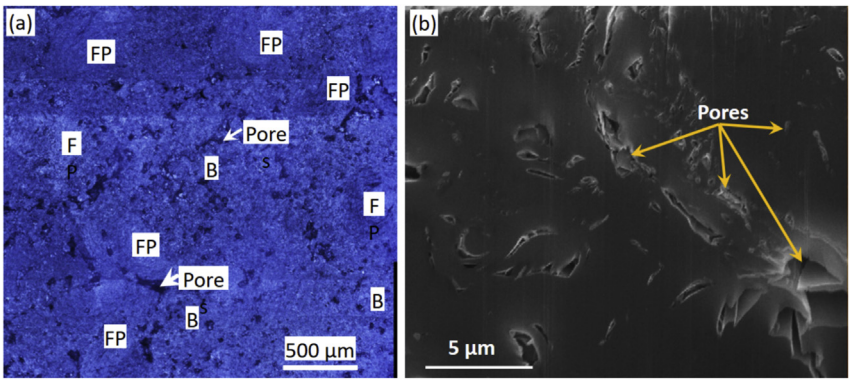

Fig. 1. (a) Optical image of Gilsocarbon graphite microstructure showing filler particles (FP), binder phase (B) and macro-size pores. Only a few of the FP are labelled for reference; (b) a scanning electron microscopy (SEM) image of a focussed ion beam (FIB) milled cross-section from the binder phase [7].

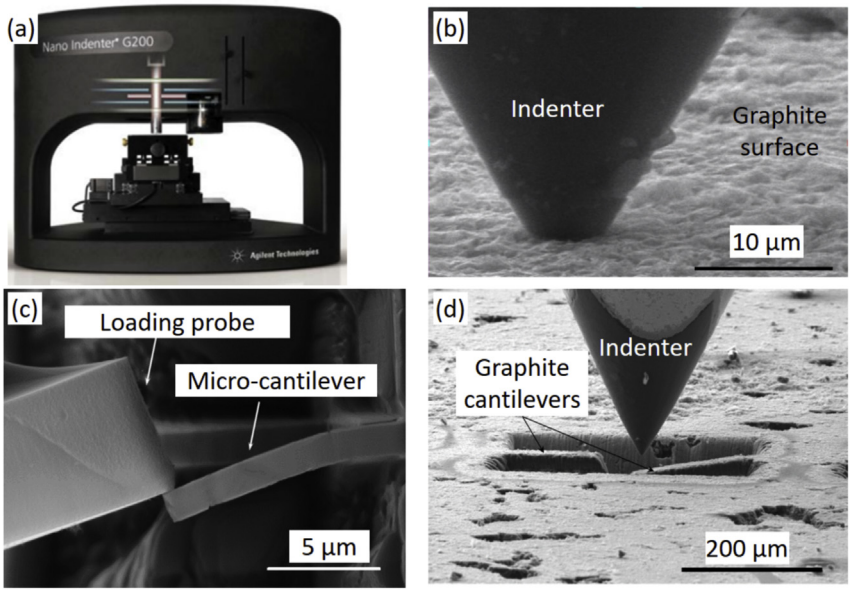

Fig. 2. The four types of rigs used in the micro-mechanical testing: (a) *ex situ* test using a standard G200 nano-indenter with an optical microscope; (b) *in situ* test using an Asmec nano-indenter (Zwick/Roell) located within a Zeiss AURIGA crossbeam FIB-SEM system; (c) *in situ* micro-cantilever bending of a sample with a square cross-section in a Helios NanoLab 600i Dualbeam workstation with a Kleindiek force measurement probe; (d) *in situ* micro-cantilever bending on a sample with a triangular cross-section, using the same system as in (b).

unloading-part of the curve varies from 4 to 12 GPa but those associated with shallower indentation depths, between 3000 nm and 4000 nm, give a good comparison with the known macro-scale elastic modulus values of 11–12 GPa for this material, Fig. 3b. The hardness, when plotted as a function of the indentation depth, reveals that it is at the softer positions (which produce greater penetration depths) where the values become extremely low (Fig. 3b).

To understand and visualise the indentation process, *in situ* nano-indentation in an SEM chamber was undertaken, with example results shown in Fig. 3c–e. As the indenter was moved through a sequence of programmed locations at fixed intervals, the load-displacement curve was observed to change with the local microstructure as the material was not homogeneous. When the indenter samples a flat and 'solid' region, a standard load-displacement curve is produced (Fig. 3c) giving a Young's modulus value of about 10 GPa. However, on many occasions, when a pore is encountered, either directly below the indenter or close to the indented region, the load-displacement curve is modified, as seen in Fig. 3d and e, leading to a large indentation depth and lower modulus.

3.2. Cantilever bend tests

3.2.1. Micro-cantilevers

Briefly, the results from the 'small' cantilever beams (~2 × 2 µm cross-section) are reviewed here but the detailed measurements can be found in Ref. [7]. An example of a load-displacement curve is given in Fig. 4a. The elastic modulus, E, is determined from the load-displacement curve:

$$E = PL^3 \Big/ 3\delta I \tag{1}$$

Where P is the load, L is the loading arm length measured from the loading point to the fixed end, δ is the deflection at the loading point and I being the moment of inertia. For a beam with squared cross-section of the dimension $a \times a$, the moment of inertia can be described as:

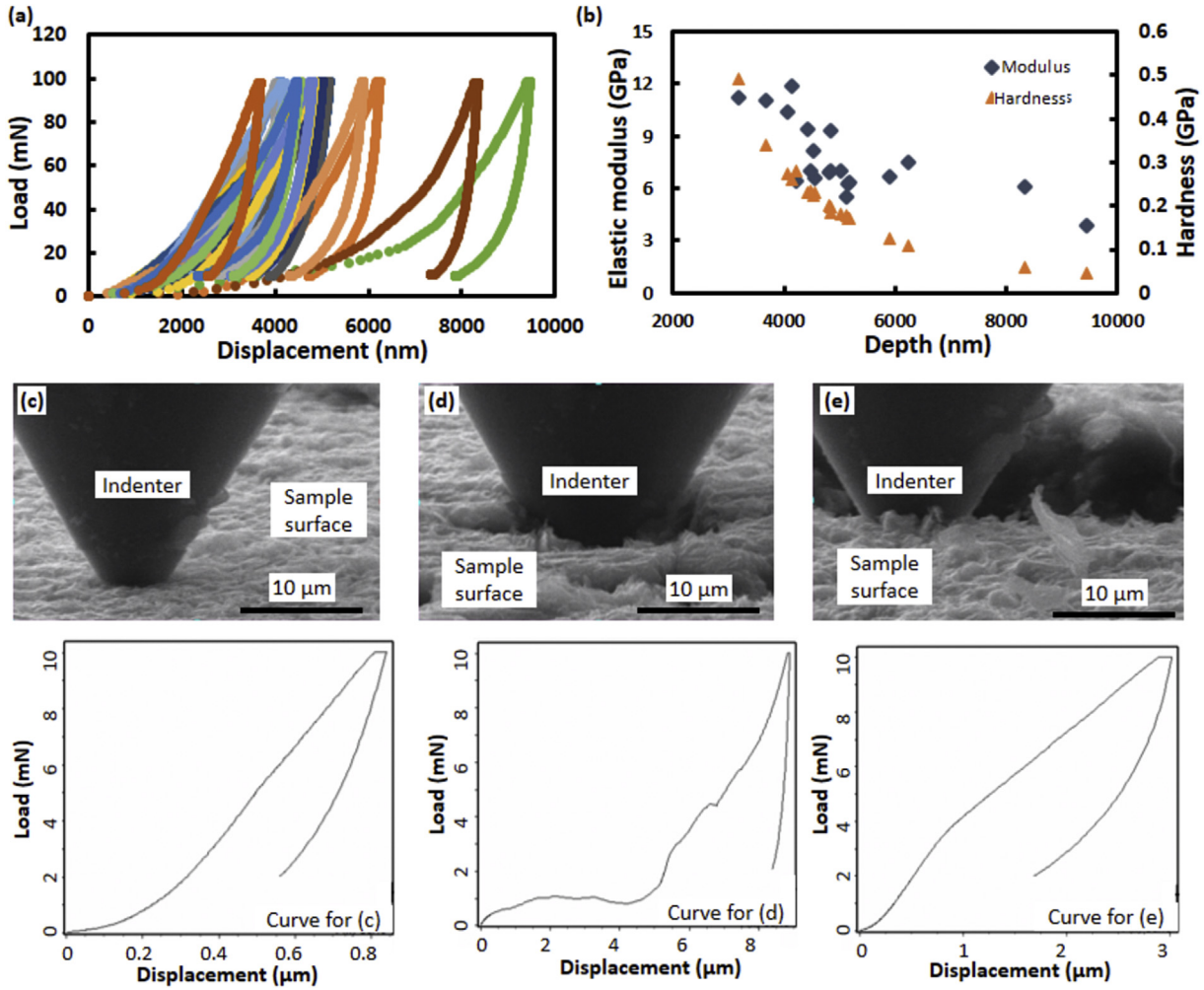

Fig. 3. (a) *Ex situ* indentation load-displacement curves from 20 different locations; (b) the elastic modulus and hardness data extracted from the *ex situ* indentation tests change with indentation depth; (c–e) *In situ* nano-indentation inside an SEM showing the corresponding load-displacement curve when (c) a flat and seemingly pore-free material is sampled, (d) the indenter intersects a large pore and (e) the indented region is close to a large pore.

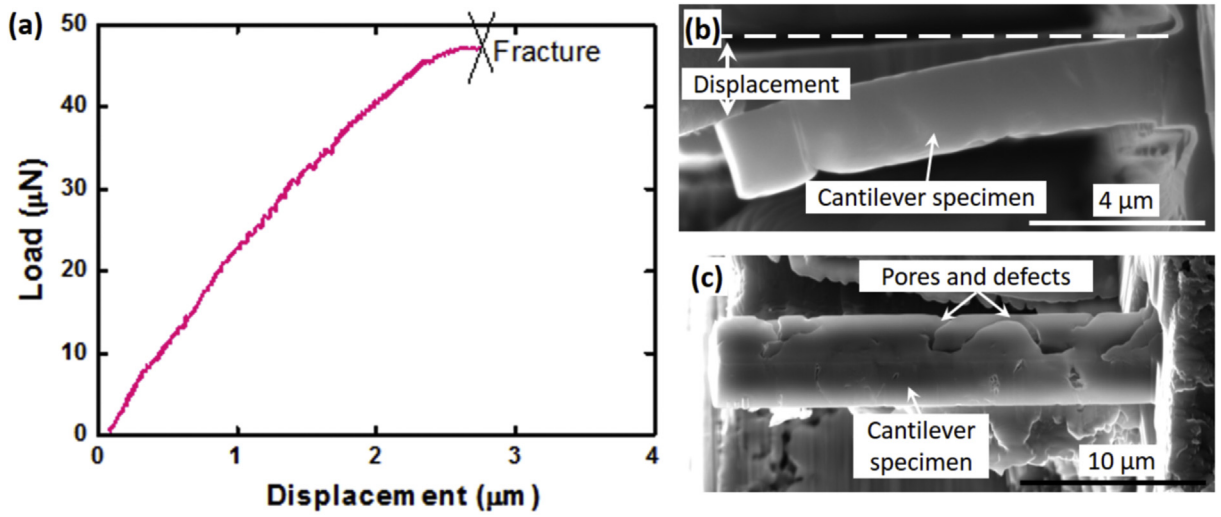

Fig. 4. (a) Load-displacement curve for a cantilever with less surface defects showing the linear and non-linear stages prior to fracture; (b) and (c) are typical cantilevers at this length-scale with varied surface defects that lead to scatter in the measured modulus and strength.

$$I = a^4/12 \quad (2)$$

These small micro-cantilever beam test specimens (Fig. 4b) showed strengths that varied from very low (some of the specimens failed prior to loading due to the presence of large defects) to very high: as much as 1000 MPa with an elastic modulus of about 67 GPa for cantilevers with no obvious surface defects. One additional point worth raising is that, the small micro-cantilevers presented in this work were typically 2 × 2 μm in cross-section size and therefore provide a measure of the true properties, but are still dependent on the presence of local micro-scale and sub-micrometre pores (Fig. 4c). It is the different proportions of such porosity that introduce scatter to the acquired data.

3.2.2. Meso-cantilevers

Five meso-scale cantilever specimens, one order of magnitude larger in size (~20 × 20 × 150 μm) compared with the micro-scale cantilever beams in the previous section and those described in Ref. [7], were tested *in situ* inside an SEM (Fig. 5a). After fracture, the specimens were transferred to a Helios NanoLab 600i Dual-beam workstation to characterise the fracture paths (Fig. 5b) while FIB milling was used to measure the cross-section size (Fig. 5c). It can be seen that the side surface of the cantilevers created by laser ablation is relatively smooth and the porosity is visible (Fig. 5d).

Comparing Fig. 5d and Fig. 4b and c, the larger population of the micro-pores contained in the meso-scale specimens should ensure that the measured properties represent an average for the micro-porous graphite. These cantilevers have a triangular cross-section as shown in Fig. 5c. For each test specimen, multiple loading cycles were applied, and the slope of the first 15% of the unloading curve was used to calculate the elastic modulus (Fig. 5e). As the cantilevers have a triangular cross-section, the moment of inertia around axis x_c, is:

$$I = bh^3/36 \quad (3)$$

Where b and h are the width and height of the cross-section respectively as marked in Fig. 5c (x_c and y_c represent the rotation axes at the centre of the sample).

In general, there are three stages in the load-displacement curve: firstly a linear-elastic stage where upon removal of the load there was no residual permanent displacement. This is followed by a pronounced non-linear stage prior to peak load with no obvious crack formation at the specimen surface but with a permanent displacement introduced upon unloading. The final stage is the 'graceful' failure after peak load where the load drop is gradual and accompanied by progressive fracture in the specimen. The elastic moduli calculated from the five specimens are 19 GPa, 23 GPa, 21 GPa, 20 GPa and 22 GPa. Due to the large deformation and significant amount of non-linearity prior to peak load, the fracture strength of the material is an approximation when using beam theory. However, taking the load at which the deformation changes from linear to non-linear (yielding), and calculating the proportional limit, σ_p, using

$$\sigma_p = FL/Z \quad (4)$$

Where Z is the section modulus. It gives corresponding values of 78 MPa, 81 MPa, 66 MPa, 72 MPa and 82 MPa. Typically at the limit of proportionality, strain for all the specimens was on average about 0.3%. Note that as reported by other authors, a strain of 0.2% for tests undertaken at the macro-scale would have already led to fracture while at the micro-scale this strain only takes graphite just beyond the proportional limit. The actual fracture strain, measured at the peak load, in the current meso-scale specimens was up to 1%.

In addition, the unloading elastic modulus decreases with increased applied peak load (Fig. 6). Here all of the results from the five samples tested are plotted where the unloading elastic modulus of each cycle is a function of the ratio between peak load of the cycle versus the final peak load where failure occurred. Two of the specimens were subjected to two loading cycles and thus only one modulus value was obtained from the first unloading cycle. This decreasing modulus with increasing peak load indicates that prior to the formation of a large crack at the start of failure, small micro-cracks develop within the volume of deformed material. Thus the unloading modulus decreased and a permanent displacement was often observed upon complete removal of loading (Fig. 5e). As it is an *in situ* approach that has been adopted, we found that the large crack forms at the peak load of the load-displacement curve and as the crack propagates, the load decreases progressively to form the 'graceful' failure as shown in Fig. 5e. Prior to this final cycle, the permanent displacement after each loading cycle was considered to be caused mainly by unrecoverable micro-cracking that is not visible on the surface of the specimen. The energy dissipated during the micro-cracking process is reflected in the area between the loading and unloading curves during each loading cycle (Fig. 5e).

It is worth noting that for both the small cantilevers (tested using Kleindiek probe) and meso-cantilevers (tested using Asmec in-SEM indenter), the fractured cantilever beams would invariably return close to its horizontal position upon removal of the loading force – even after the graceful failure post peak load. Fig. 7 shows an example where the cantilever was loaded to fracture. It was evident that the crack propagated through more than 90% of the beam cross-section and the path was tortuous. When the indenter was retracted from the specimen (Fig. 7a), the cantilever slowly restored its position close to horizontal (Fig. 7b), and the crack closed. The same scenario was observed in all the cantilevers, although in some cases the crack closed only partially. We did not obtain direct evidence, such as TEM imaging, of what actually happened at the crack tip region to allow the cantilever to bounce back, but we propose a tentative explanation. For all the specimens tested, a tortuous crack path was followed creating two fracture surfaces keying into each other, which allowed the crack to propagate in a stable and controlled manner. In the meantime, the deformed region ahead of the crack tip is still in the elastic regime and relaxes to its original state upon removal of the load. Considering the nature of the layered structure of graphite, it is also possible that sliding between the layers accommodated elastic deformation that is recovered when the external load is removed. Indeed, the stress state at the root of a bent cantilever is complex, especially when the crack extends beyond the neutral axis, but this bounce-back scenario occurred also to specimens with shorter cracks (above the neutral line). Therefore, we consider this large recoverable elastic strain ahead of the crack front as a typical micro-scale deformation mechanism for nuclear graphite; which is also consistent with the large yield strain measured in material at this length-scale. Such phenomenon has not been observed in macro-scale tests.

4. Discussion

The results acquired at the meso-scale in the present work are compared with micro-scale data and macro-scale data obtained by the present workers as well as from other studies from the literature performed on the same batch of Gilsocarbon graphite (Fig. 8). Gilsocarbon is a material with pores covering multiple length-scales from nanometres to millimetres in size. The region between the macro-pores is material that contains micro- and nano-

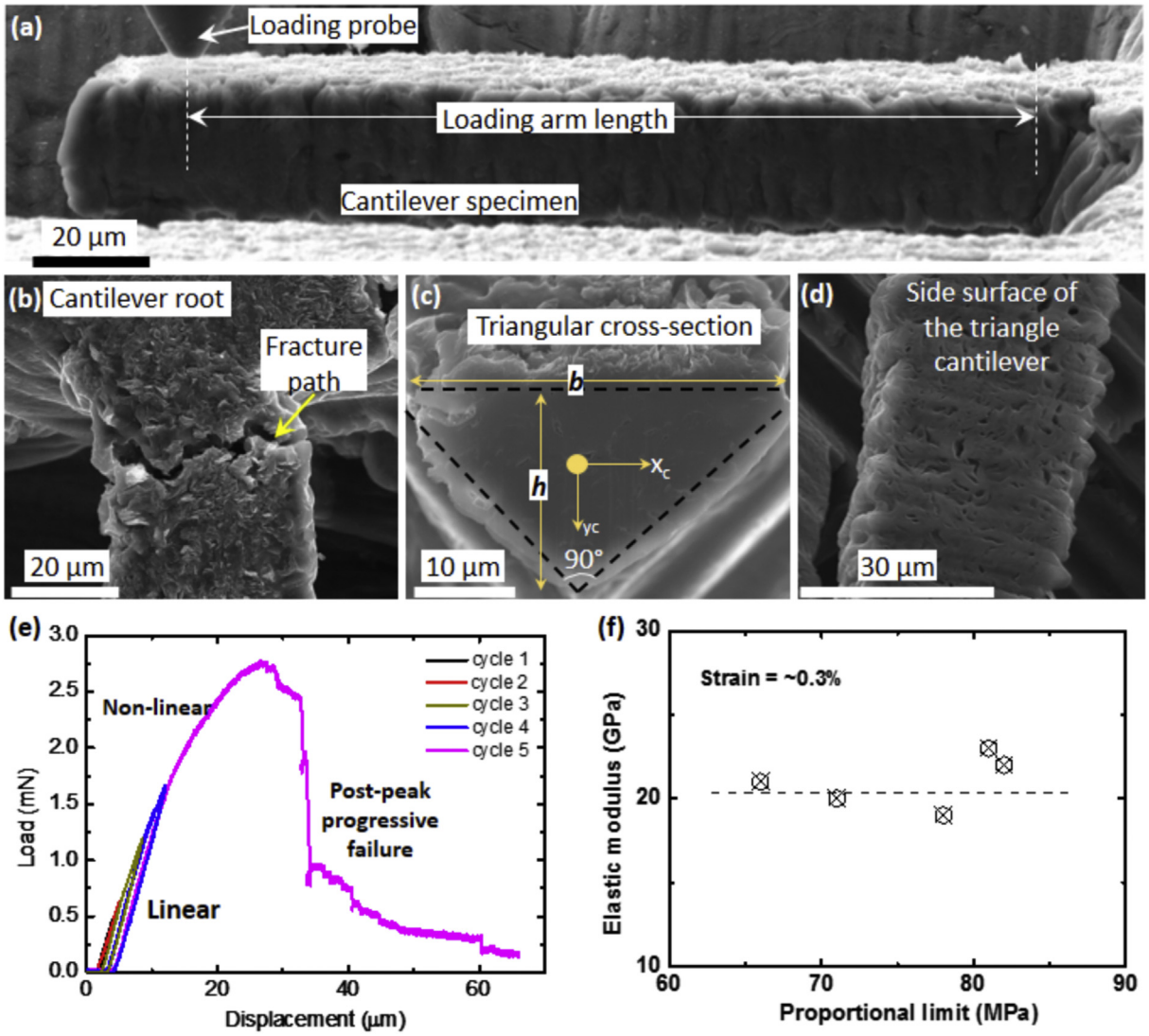

Fig. 5. (a) SEM image of a cantilever before a loading cycle showing the relative position of the indenter, the loading arm length and the root of the specimen; (b) top surface of the specimen showing the tortuous fracture path close to the root; (c) a FIB milled cross-section of the fractured cantilever; (d) the side surface of the cantilever revealing the distribution of micro-pores; (e) a typical load-displacement curve for multiple loading cycles showing the linear, non-linear and post-peak progressive failure stages, and (f) the elastic modulus versus the proportional limit for all the five specimens tested.

sized pores. At the micro-scale, since the cross-sections of the cantilever specimens are below a few micrometres, samples are free from micro-pores and surface defects and therefore provide representative graphite properties. At this length-scale, the highest elastic modulus value measured was about 67 GPa (see Ref. [7]). However, a large scatter is introduced to the measured data as a result of the small volume of material sampled. Increasing the cantilever specimen size by one order of magnitude to the meso-scale with cross-sections of about 20 × 20 μm, the value for elastic modulus obtained from the five test specimens averaged about 21 GPa with a standard deviation of 1.5 GPa. Certainly, these specimens sampled material that excluded the large macro-pores to evaluate the properties of graphite containing micro- and nano-pores.

Fig. 8 summarises elastic modulus values obtained from the micro-scale to conventional laboratory centimetre sized samples. The transition region 3 includes the possibility that when macro-pores (either globular gas bubbles in the binder phase or lenticular pores along the circumference of filler particles) cut through the meso-scale specimens, this will result in a lower ratio of strength/elastic modulus, although in the five specimens tested here, no such macro-pores were intersected. The laboratory size test data (region 2) reported in the literature give the modulus to be between 11 and 12 GPa with a reduced scatter. This is similar to the *in situ* indentation data obtained from 'good' areas on the graphite surface which centres around 10–13 GPa. Considering the *ex situ* indentation data shown in Fig. 3b which changes from about 12 GPa to as low as 4 GPa, it indicates that these data fall into the 'macro-scale' regime in Fig. 8. Although nano-/micro-indentation tests are known to sample a relatively small local volume of materials, in this nuclear graphite there is the potential for the results generated by indentation to be influenced by the presence of large pores; hence relatively low elastic modulus values were measured (Fig. 3). The micro-scale specimens in region 1 (Fig. 8) show a large scatter, depending upon whether no micro pores or many were contained by each specimen. The elastic modulus of a material is not very sensitive to processing, geometry or microstructure. The obviously changing modulus in Gilsocarbon graphite is consistent with this

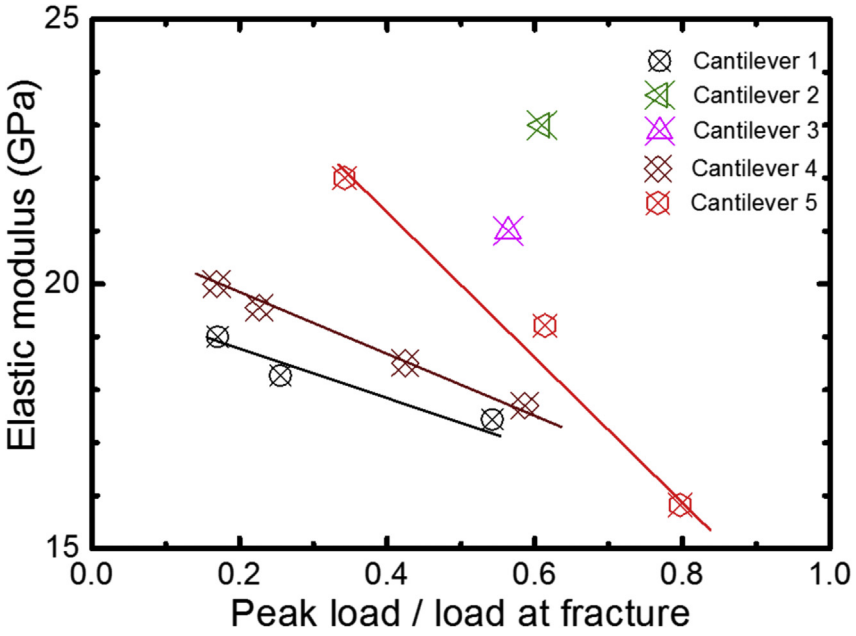

Fig. 6. Elastic modulus decreases with increased peak load.

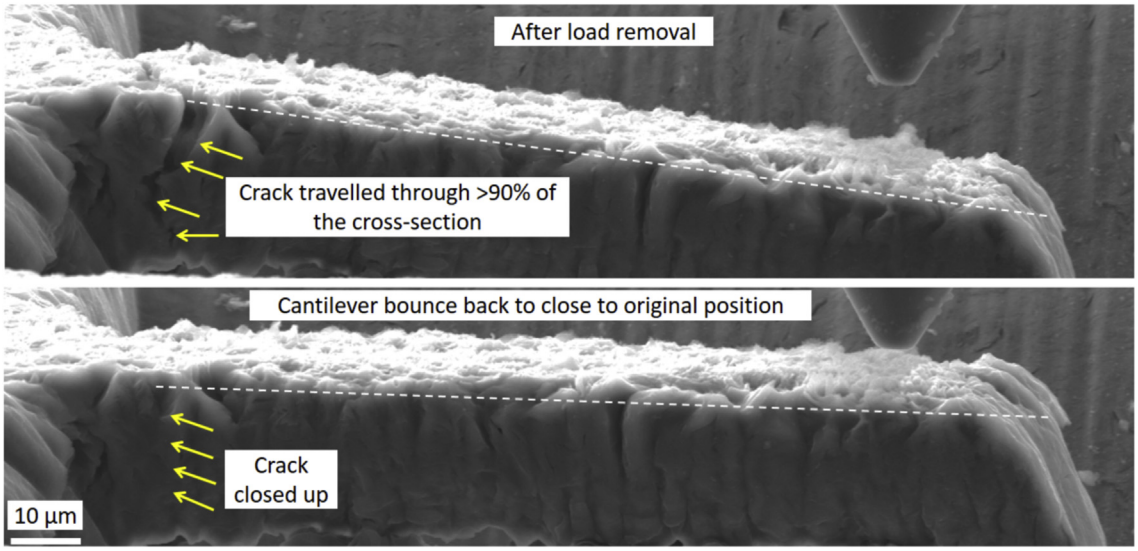

Fig. 7. Images of the cantilever bounce back after the removal of load (a) and subsequent crack closure (b) despite the presence of a crack larger than 90% of the cross-section.

statement but the data in Fig. 8 also indicates that it is a different material, or rather structure, that has been sampled and tested at each length-scale. Here we have referred to only the elastic modulus change with specimen size but the flexural strength has a similar trend – the details of which can be found in Ref. [7].

These experimental results have implications for modelling. One example of a numerical model is that proposed by Rose and Tucker [19] which combines weakest link theory from Weibull analysis and a fracture mechanics approach. For this and similar models, there are usually two important inputs: (i) a simplified, experiment-based characterization of the microstructure to represent the main features of the material such as the size and distribution of the filler particles and pores that develop over the period of service and (ii) the mechanical properties for the constituent elements. Both of these must consider the scales in terms of the 2D length or 3D volume of the model that is adopted. Each model requires input data acquired to represent the basic linear elastic material, namely at the micro-scale when the material is ideally flaw-free.

Consideration of size effects is usually related to the number of crack initiation sites sampled by a given size test specimen. In general, for a material with a homogeneous microstructure the measured property changes are associated with the population of local defects. However, nuclear graphite is a more extreme case because as specimen size is increased, different features of the bulk material are sampled so that the ultimate properties measured will be influenced by different microstructural features and mechanisms. For example, in macro-scale specimens (>a few millimetres), the macro-pores (a few hundred micrometres in diameter) play the primary role in controlling the measured property. To

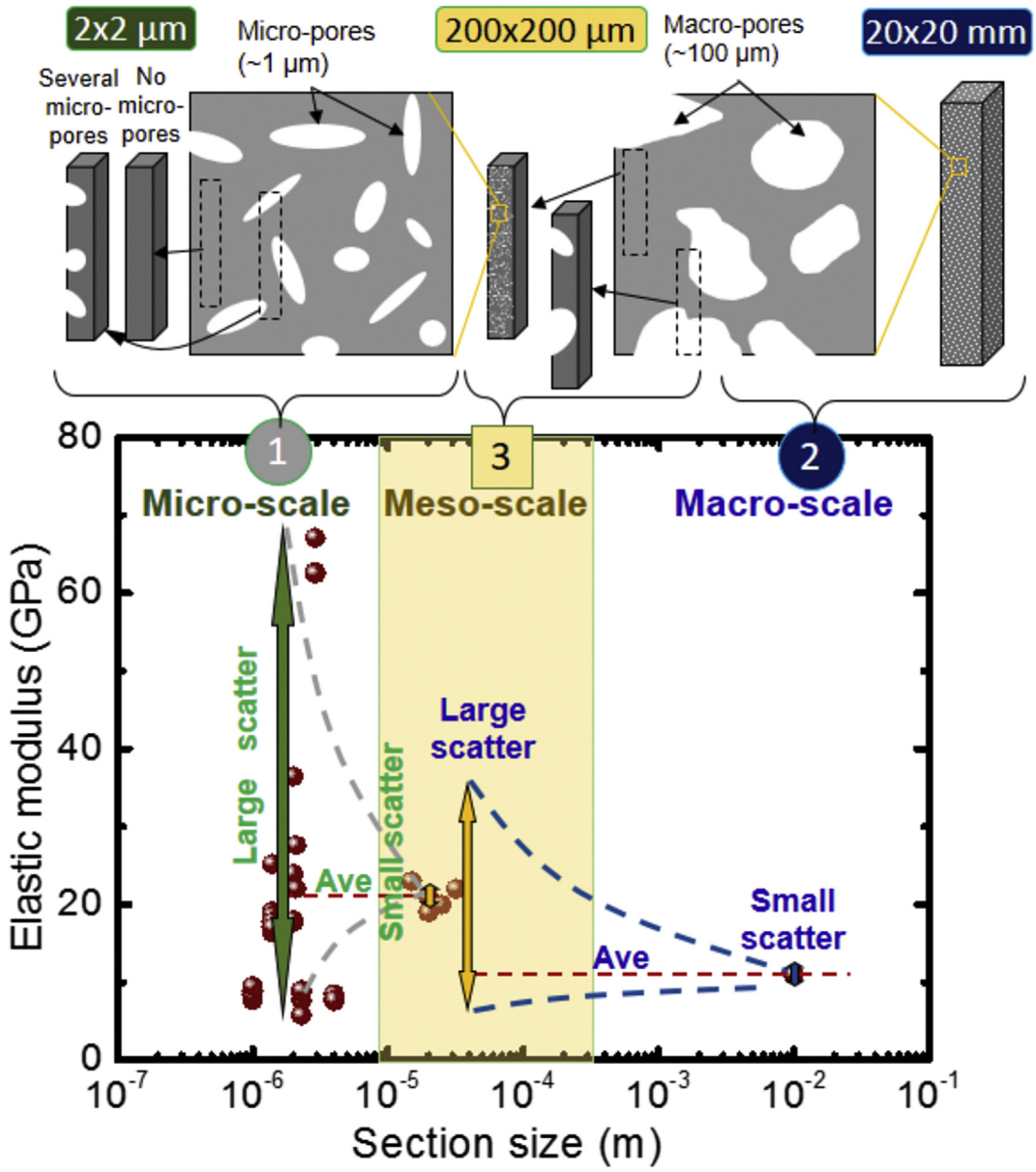

Fig. 8. Elastic modulus changes with the cross-section size (regions 1, 2 and 3) of test specimens for Gilsocarbon graphite.

model this level of detail it is necessary to capture the microstructure of graphite at all length-scales, and this made it impossible to numerically model it using a single length-scale approach. Therefore, models have been developed that take into account the complex microstructure of nuclear graphites including the filler particles, the matrix and porosity; for example, Savija *et al* [5]. That particular model is a 3D multi-length scale finite beam element model that addresses the elastic properties together with deformation and fracture of porous quasi-brittle materials. The microstructure that is invoked can be based on either synthetic simulations or X-ray computed tomographic images. It accommodates pore size distributions across the macro- and micro-length-scale. Measurement of the input parameters of elastic modulus and fracture strength have to be made at the appropriate length-scale; frequently the micrometre length-scale. As a consequence it is possible to predict the contributions of porosity to the elastic modulus, deformation and fracture strength at different length-scales. With such a model it was found that the micro-size pores affect the macro-scale strength primarily; replacing 20 vol% of macro-pores with 20 vol% of micro-pores in a sample with 40 vol% total porosity, the elastic modulus would increase from 50% of the pore-free value to 23%.

In terms of the mechanical behaviour between micro-scale (Fig. 4 and Ref [7]) and those tested by bending a larger cantilever of an order of magnitude larger (Figs. 5–7), there are several similarities and differences. The micro-scale failure depends largely on the distribution of micro-pores (compare Fig. 4b and c) hence large scatter in measured data. For the meso-scale cantilevers, due to the relatively large population of micro-scale pores, their distribution had less impact on the final results and potentially allowed more micro-cracks to occur and coalesce before final fracture (note the pronounced non-linearity prior to peak load), Fig. 5e. As a consequence, more prominent softening curves are observed representing progressive failure within the test volume. Nano-indentation tests, on the other hand side, are difficult to quantify due to the complex stress state and the presence of pores

at different length-scales. In general, to obtain a reliable evaluation of the mechanical properties in nuclear graphite, creating free-standing specimens such as cantilever beams is considered as a realistic test method.

A final point on the failure strain in these micro and macro-cantilevers: it is noteworthy that at the micro-scale, the specimens deform more than at the macro-scale. As reported by other workers [7,16,20], who investigated a similar Gilsocarbon graphite, usually a 0.2–0.3% failure strain was measured for laboratory size specimens. However, in the micro-scale testing, for the large cantilever, 0.3% strain extends just beyond the linear-elastic range. The final elongation at fracture is much higher up to nearly 1% for the meso-sized specimens. This indicates that the millimetre size pores in the macro-specimens play an important role in controlling the degree of brittleness for these materials. This explains that although graphite is termed as a 'quasi-brittle' material, the macro-scale load-displacement curves have a very short non-linear stage prior to the peak load and this is often followed by more abrupt fracture rather than progressive graceful failure observed at the micro-scale.

5. Conclusions

The testing of Gilsocarbon graphite specimens at micro-scale and meso-scale were investigated and compared with macro-scale data. It was found that:

- The elastic modulus decreases from 67 GPa to 11 GPa as the specimen cross-section size was increased from several micrometres to several centimetres. A similar trend was measured in flexural strength.
- At the micro-scale and meso-scale, the specimens tend to have a higher failure strain compared with those tested at the macro-scale.
- The millimetre-size pores are considered to contribute to the 'brittleness' of the Gilsocarbon graphite specimens at the macro-scale.
- It is emphasized here that for materials with complex multi-scale microstructural features, a multi-scale approach has to be undertaken, preferably using *in situ* techniques allowing the correlation between properties and microstructure. Care has to be taken when using *ex situ* experimental techniques such as indentation and the data are not always representative without considering the local microstructures.

Acknowledgment

DL acknowledges the EPSRC postdoctoral fellowship grant: EP/N004493/1 (An innovative, multi-scale, real-time approach to the understanding of deformation and fracture in irradiated nuclear reactor core graphites) and the Royal Commission for the Exhibition of 1851 Research Fellowship Award. DL and PEJF acknowledge the ESPRC grant: EP/J019801/1. NPL acknowledges funding by the Department for Business, Energy and Industrial Strategy. This work was also supported by a Natural Environment Research Council fellowship awarded to OTL at Bristol (NE/J018945/1). DL thanks Dr. Chris Hardie (UKAEA Culham) for help on the indentation test using G200.

References

[1] D. Liu, S. Nakhodchi, P. Heard, P.E.J. Flewitt, Graph. Test. Nucl. Appl. Significance Test Specim. Vol. Geom. Stat. Significance Test Specim. Popul., vol. STP1578, no, in: Nassia Tzelepi, Mark Carroll (Eds.), Small-scale Approaches to Evaluate the Mechanical Properties of Quasi-brittle Reactor Core Graphite, 2015, pp. 1–21.
[2] P.J. Heard, M.R. Wootton, R. Moskovic, P.E.J. Flewitt, Crack initiation and propagation in pile grade A (PGA) reactor core graphite under a range of loading conditions, J. Nucl. Mater. 401 (1–3) (2010) 71–77.
[3] B.J. Marsden, et al., Dimensional change, irradiation creep and thermal/mechanical property changes in nuclear graphite, Int. Mater. Rev. 61 (3) (2016) 155–182.
[4] Z. Zhou, et al., From nanopores to macropores: fractal morphology of graphite, Carbon 96 (2016) 541–547.
[5] B. Šavija, D. Liu, G. Smith, K.R. Hallam, E. Schlangen, P.E. Flewitt, Experimentally informed multi-scale modelling of mechanical properties of quasi-brittle nuclear graphite, Eng. Fract. Mech. 153 (2015) 360–377.
[6] T.J. Marrow, et al., In situ measurement of the strains within a mechanically loaded polygranular graphite, Carbon 96 (2016) 285–302.
[7] D. Liu, P.E.J. Flewitt, Deformation and fracture of carbonaceous materials using in situ micro-mechanical testing, Carbon 114 (2017) 261–274.
[8] R. Krishna, A.N. Jones, L. McDermott, B.J. Marsden, Neutron irradiation damage of nuclear graphite studied by high-resolution transmission electron microscopy and Raman spectroscopy, J. Nucl. Mater. 467 (2015) 557–565.
[9] P.J. Heard, M.R. Wootton, R. Moskovic, P.E.J. Flewitt, Deformation and fracture of irradiated polygranular pile grade A reactor core graphite, J. Nucl. Mater. 418 (1–3) (2011) 223–232.
[10] D. Liu, P. Heard, B. Šavija, G. Smith, E. Schlangen, P. Flewitt, Multi-scale characterization and modelling of damage evolution in nuclear Gilsocarbon graphite, MRS Proc. 1809 (2015) 1–6.
[11] J.S. Field, M.V. Swain, The indentation characterisation of the mechanical properties of various carbon materials: glassy carbon, coke and pyrolytic graphite, Carbon 34 (11) (1996) 1357–1366.
[12] D.E.J. Armstrong, A.J. Wilkinson, S.G. Roberts, Measuring anisotropy in Young's modulus of copper using microcantilever testing, J. Mater. Res. 24 (11) (2009) 3268–3276.
[13] D. Kiener, C. Motz, G. Dehm, Dislocation-induced crystal rotations in micro-compressed single crystal copper columns, J. Mater. Sci. 43 (7) (2008) 2503–2506.
[14] J.E. Darnbrough, D. Liu, P.E.J. Flewitt, Micro-scale testing of ductile and brittle cantilever beam specimens in situ with a dual beam workstation, Meas. Sci. Technol. 24 (5) (2013) 55010.
[15] J.E. Brocklehurst, M.I. Darby, Concerning the fracture of graphite under different test conditions, Mater. Sci. Eng. A 16 (1–2) (1974) 91–106.
[16] Z. Mileeva, D.K. Ross, S.M. King, A study of the porosity of nuclear graphite using small-angle neutron scattering, Carbon 64 (2013) 20–26.
[17] Y. Vertyagina, T.J. Marrow, Multifractal-based assessment of Gilsocarbon graphite microstructures, Carbon 109 (2016) 711–718.
[18] G.M. Laudone, C.M. Gribble, G.P. Matthews, Characterisation of the porous structure of Gilsocarbon graphite using pycnometry, cyclic porosimetry and void-network modeling, Carbon 73 (2014) 61–70.
[19] A.P.G. Rose, M.O. Tucker, A fracture criterion for nuclear graphite, J. Nucl. Mater. 110 (2–3) (October 1982) 186–195.
[20] G.M. Jenkins, The stress-strain relationships of polycrystalline graphite under compression up to fracture, Carbon 3 (1) (1965) 93–94.